All-optical multichannel logic based on coherent perfect absorption in a plasmonic metamaterial

Maria Papaioannou,[1, a)] Eric Plum,[1, b)] João Valente,[1] Edward T. F. Rogers,[1, 2] and Nikolay I. Zheludev[1, 3, c)]

[1)] *Optoelectronics Research Centre and Centre for Photonic Metamaterials, University of Southampton, Highfield, Southampton, SO17 1BJ, UK*

[2)] *Institute for Life Sciences, University of Southampton, Highfield, Southampton, SO17 1BJ, UK*

[3)] *Centre for Disruptive Photonic Technologies, School of Physical and Mathematical Sciences and The Photonics Institute, Nanyang Technological University, Singapore 637371*

The exponential growth of telecommunications bandwidth will require next generation optical networks, where multiple spatial information channels will be transmitted in parallel. To realise the full potential of parallel optical data channels, fast and scalable multichannel solutions for processing of optical data are of paramount importance. Established solutions based on the nonlinear wave interaction in photorefractive materials are slow. Here we experimentally demonstrate all-optical logical operations between pairs of simulated spatially-multiplexed information channels using the coherent interaction of light with light on a plasmonic metamaterial. The approach is suitable for fiber implementation and — in principle — operates with diffraction-limited spatial resolution, 100 THz bandwidth and arbitrarily low intensities, thus promising ultrafast, low-power solutions for all-optical parallel data processing.

Encoding, transmitting, harvesting and processing information in the spatial domain is anticipated to be the next breakthrough in the hunt for technologies that will overcome the forthcoming capacity crunch[1,2]. Research advances in the field of multi-core and multi-mode fiber design and fabrication have flourished over the past few years, providing numerous efficient routes to data transfer in spatially multiplexed channels[3–5]. However, in order to exploit the capacity increase of spatial optical parallelism, new data processing schemes are needed. Established electronic solutions have high energy requirements and complexity as they require conversion between optical and electronic signals, while all-optical techniques enabled by photorefraction are slow. Recently, several metamaterial-based approaches to dynamic spatial control over optical signals have emerged[6–8], including all-optical ones[9,10], which create interesting possibilities.

Here, we propose a data processing platform based on the interaction of photons at metamaterial beam splitters (see Fig. 1(a)). In general, beam splitters may be either lossless or lossy and are fundamental components of many systems in both classical and quantum optics. Considering illumination by a single beam of light, we define the limiting case of an *ideal lossless beam splitter* as an interface having 50% transmission and 50% reflection, and the limiting case of an *ideal lossy beam splitter* as an interface having 25% transmission, 25% reflection and 50% absorption, i.e. the largest possible absorption for truly planar structures[11]. In this manuscript, we explore the optical data processing capability of lossy beam splitters in the classical regime. The underpinning principle[12–16] enables all-optical control over light-matter interactions

and it was recently shown to allow complete suppression and enhancement of absorption of light by lossy beam splitters (planar metamaterials)[17] with diffraction-limited spatial resolution[10].

An ideal lossy beam splitter can be realized by a planar metamaterial, as these structures allow precise engineering of their transmission, reflection and absorption characteristics. A planar metamaterial is a periodically structured film of substantially sub-wavelength thickness and its optical properties are controlled by the constituent material(s) and the geometry of its (sub-wavelength sized) unit cell[18]. Using a thin plasmonic metamaterial as our lossy beam splitter, we apply spatially-selective absorption of light to simple representations of spatially multiplexed signals in free-space, demonstrating all-optical Boolean logic operations between such information channels. This type of linear interaction between coherent light beams has been shown to operate on a femtosecond timescale by Refs. 19 and 20, and it is thus much faster than techniques based on the slow microsecond to second scale photorefractive nonlinearity[21–26], which also allow all-optical dynamic wavefront shaping. In contrast to nonlinear techniques in general, our approach is linear and therefore does not have fundamental minimum intensity requirements. Moreover, the scheme could be implemented in a multi-core fiber network and extended to additional degrees of control since interaction of coherent waves on metamaterials also allows the polarization[27] and propagation direction[28] of optical signals to be modulated at single-photon intensity levels[29].

Our approach is based on the interaction of counter-propagating coherent waves on an absorbing beam splitter of substantially sub-wavelength thickness. Counter-propagating coherent copolarized electromagnetic waves form a standing wave consisting of electric field anti-nodes and nodes separated by a quarter of a wavelength. A sufficiently thin film can be placed at such a position of constructive or destructive interference, leading to en-

---

[a)]Electronic mail: mcp1g13@soton.ac.uk

[b)]Electronic mail: erp@orc.soton.ac.uk

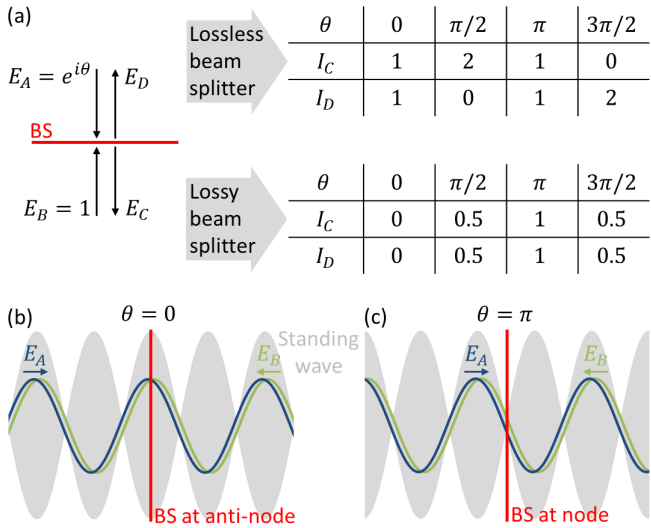[c)]Electronic mail: niz@orc.soton.ac.uk; www.nanophotonics.org.uk

FIG. 1. **Interaction of coherent light beams on lossless and lossy beam splitters.** (a) The output intensities, I_C and I_D, depend on the phase difference $\theta = \arg E_A - \arg E_B$ between the equal intensity input beams, $I_A = I_B = 1$, on the beam splitter (BS), where the intensity I_i corresponding to the electric field E_i is defined as $I_i = |E_i|^2$. For the lossy beam splitter we consider the "ideal" case providing 50% single beam absorption and 25% single beam transmission and reflection each. (b) Constructive interference of electric fields E_A and E_B on the beam splitter results in enhanced electric light-matter interaction and coherent perfect absorption in the lossy case. (c) Destructive interference of electric fields on the beam splitter prevents the electric light-matter interaction, rendering the beam splitter perfectly transparent.

hancement or suppression of the electric light-matter interaction, see Fig. 1(b) and (c) respectively. We note that the magnetic field of normally incident plane waves cannot couple to a truly planar metasurface or metallic thin film[30,31] as such structures cannot support in-plane magnetic dipole excitations (and their higher order combinations) due to all charges being confined to a single plane[32]. Therefore, absorption is negligible at the electric field node, while absorption of up to 100% is possible at the electric field anti-node. Thus, the intensity and phase of one wave control the absorption of the other, allowing modulation of light with light without nonlinearity[17] in a way that corresponds to elementary all-optical logical operations. As coherent control of absorption from 0% to 100% requires an ideal lossy beam splitter, such a structure is also known as coherent perfect absorber. An ideal lossy beam splitter exhibits identical optical properties for opposite directions of illumination and absorbs 50% of a single illuminating beam. For illumination by coherent counterpropagating waves, input intensities (I_A and I_B) and output intensities (I_C and I_D) are related by

$$I_C = I_D = (I_A + I_B - 2\sqrt{I_A I_B} \cos\theta)/4, \qquad (1)$$

where θ is the phase difference between waves A and B at the ideal lossy beam splitter [see equation (5) of Ref. 33

with parameter $s = -0.5$]. While absorption of 100% for $\theta = 0$ and 0% for $\theta = \pi$ require $I_A = I_B$, we note that tolerance towards input intensity differences is large, e.g. if one input intensity is twice as large as the other the absorption levels only change marginally to 97% and 3%, respectively.

In this proof-of-principle experimental demonstration we employ simple binary intensity profiles to simulate spatially multiplexed signals. We consider a signal that is composed of 5 spatially separated circular intensity lobes that could represent separate information channels running along a multi-core fiber, Fig. 2(i). These are combined with a second set of optical channels on the metamaterial, e.g. Fig. 2(ii)-(v), to demonstrate selective logical operations on different combinations of the information channels.

Here we employ a metasurface absorber consisting of a nanostructured free-standing gold film of 60 nm thickness, which was fabricated by thermal evaporation of gold on a 50-nm-thick silicon nitride membrane, subsequent silicon nitride removal by reactive ion etching and structuring of the remaining free-standing gold film by gallium focused ion beam milling. The gold film is perforated with a $100 \times 100 \ \mu m^2$ array of split ring apertures that have an individual footprint of $350 \times 350 \ nm^2$ and a broad resonant absorption peak around 875 nm near the experimental wavelength of 785 nm. Throughout all optical experiments, the metasurface was illuminated by linearly polarized light with the electric field oriented parallel to the structure's symmetry axis. The free-standing metasurface is designed to be symmetric with respect to the light propagation direction, resulting in almost identical optical properties for opposite directions of illumination, see Fig. 2. Asymmetrically split ring aperture arrays have a rich spectrum of transmission, reflection and absorption bands discussed in Ref. 18 and our structure absorbs about 33% at 785 nm wavelength when illuminated from only one side by a single beam. Masks with holes, representing spatial information channels like those of multi-core fibers, were made by drilling holes of 0.9 mm diameter in 1 mm-thick aluminum sheets. The masks are positioned on the back focal plane of the imaging optics in beam A and beam B, aligned, and imaged onto both sides of the metasurface using light from the same 785 nm CW diode laser with 6.7 mW output power. While coherent absorption is a linear process that will work at any intensity below damage thresholds, the laser light is attenuated to few μW to avoid detector saturation. It propagates along paths of matched lengths as illustrated by Fig. 2. A standing wave forms where the metasurface is illuminated from both sides, and the position of its nodes and anti-nodes relative to the metasurface is controlled by a liquid crystal phase modulator in the path of beam B. The resulting coherent effects are detected in the output beam formed by transmission of beam A and reflection of beam B by imaging the metasurface plane onto a CCD camera. We note that 33% single beam absorption of our sample —
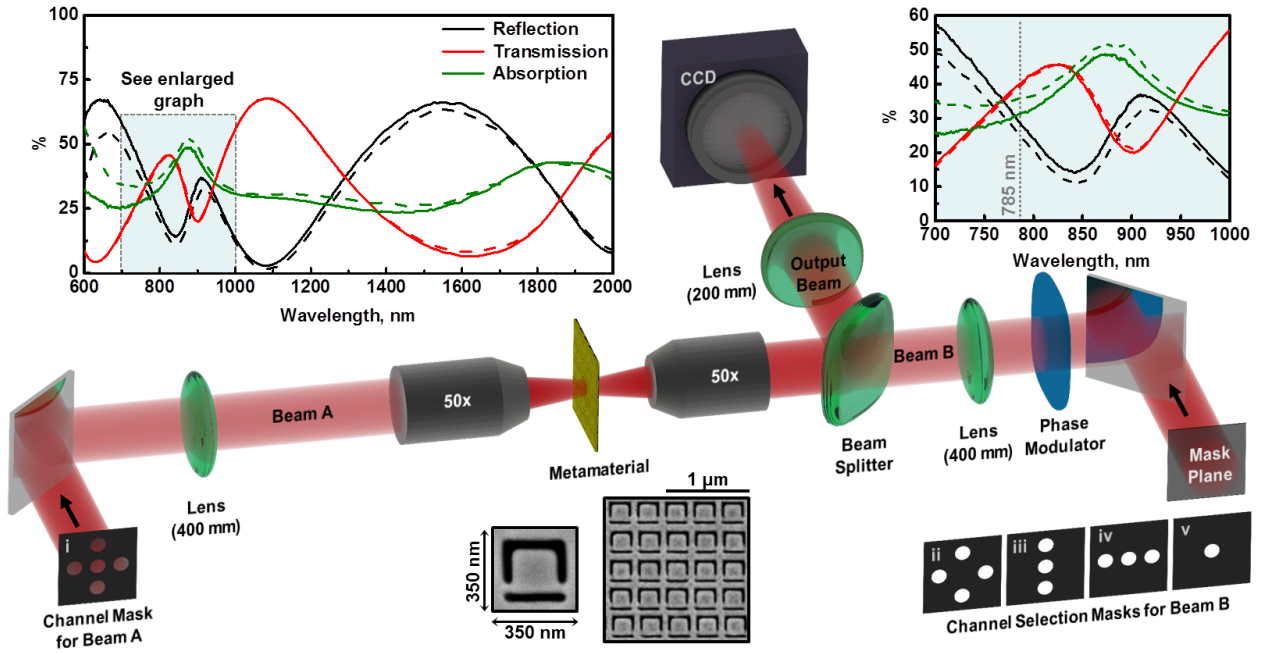
FIG. 2. **Metamaterial-based multichannel optical logic gate.** Schematic of the experimental setup where counter-propagating coherent beam profiles A and B representing information channels are imaged on the metamaterial from either side using a 400 mm focal length lens and a 50× objective to achieve 100× demagnification. The intensity profiles of beams A and B are imposed by binary masks (i-v). A phase modulator across the path of beam B controls the phase difference of the beams at the metamaterial position. The output signal is monitored by imaging the metamaterial plane onto a charge-coupled device (CCD) camera with 50x magnification using a 50× objective and a 200 mm focal length lens. Insets show spectral measurements of reflection, transmission and absorption of the free-standing gold metamaterial when illuminated from the front (solid) and rear (dashed), as well as scanning electron microscope images of a unit cell and a fragment of the metamaterial consisting of asymmetrically split ring apertures in a gold film.

rather than the ideal 50% — reduces the achievable level of coherent absorption and causes an intensity difference between the output beams, C and D[27]. The difference between experimental transmission and reflection levels is compensated for by adjusting the input intensities such that the single beam transmission of beam A and reflection of beam B have the same intensity. A metamaterial that matches the properties of an ideal lossy beam splitter more closely could be achieved by optimization of the metamaterial design and the nanofabrication conditions, for example a 10% size reduction of the nanostructure should shift the absorption peak from 875 nm to approximately the experimental wavelength of 785 nm.

All-optical logical operations result from combining coherent optical channels on the absorbing metamaterial beam splitter and externally controlling the phase difference θ_{ext} between these data channels. Thus, the phase difference θ that controls metasurface absorption is the sum of the externally imposed channel phase difference θ_{ext} and — depending on the digital modulation scheme — any phase difference θ_{data} between the interacting data bits from each channel, $\theta = \theta_{\text{ext}} + \theta_{\text{data}}$. If both interacting channel waves are in phase on the absorber ($\theta = 0$), resulting in constructive interference of electric field, the bit will be absorbed. In contrast, a phase difference $\theta = \pi$ between the channel waves results in destruc-

tive interference that renders the absorber transparent for the bit. Fig. 3 illustrates logical operations for 1 out of 5 spatial channels of beam A (panel a) with 1 phase-modulated channel of beam B corresponding to the central lobe (panel b). Consider a pair of interacting channels A and B that carry *different* coherent data streams using binary phase-shift keying (PSK). We denote the binary states that have the same intensity and a phase difference of π by "+" and "-". In-phase interaction of both phase-modulated data streams on the absorber ($\theta_{\text{ext}} = 0$) will result in suppression of absorption for opposite bits ($\theta_{\text{data}} = \pi$) which will destructively interfere on the metasurface ($\theta = \pi$, panel c) and absorption for identical bits ($\theta_{\text{data}} = 0$), which interfere constructively on the metasurface ($\theta = 0$, panel d). In comparison to the peripheral channels that were not addressed, the detected intensity of the central channel is approximately four-fold increased in the metasurface's transparent state and negligible in its absorbing state (panel e). Therefore, the result is an intensity-modulated channel corresponding to A XOR B, where high intensity corresponds to a logical "1" and low intensity corresponds to a logical "0", see Table I. The inverse logical operation can be realized by applying a constant phase shift of $\theta_{\text{ext}} = \pi$ to one channel, which eliminates the absorption of identical bits, while opposite bits are absorbed as the phase
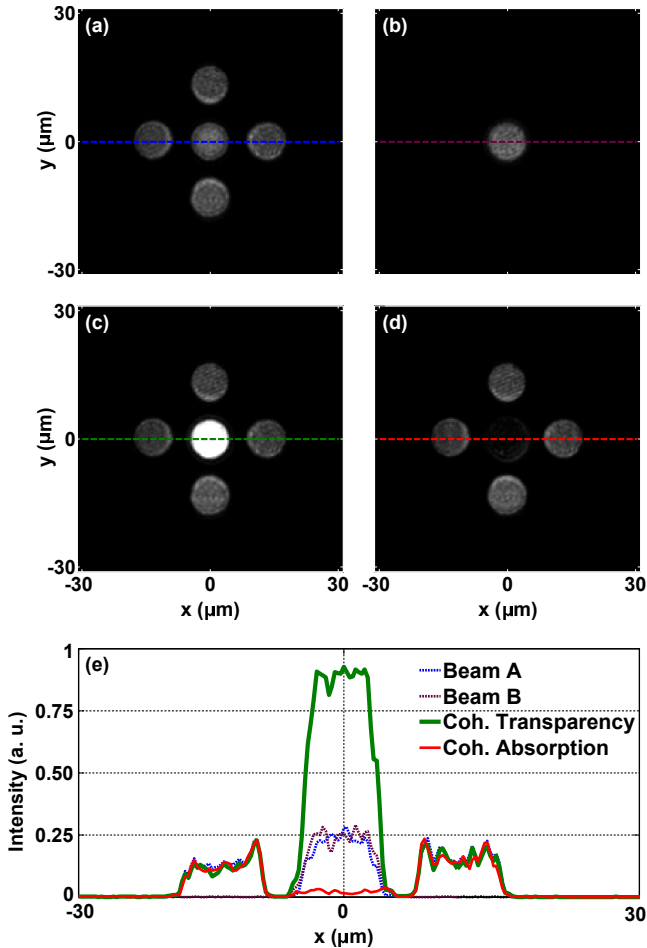
FIG. 3. **Coherent logic with the central channel.** Images of the metasurface illuminated by (a) a 5-channel signal as beam A (beam B blocked), (b) the central channel as beam B (beam A blocked), (c) beams A and B with destructive interference on the metasurface corresponding to logical operations + XOR -, - XOR + of Table I and 1 AND 1 of Table II for the central channel, (d) beams A and B with constructive interference on the metasurface corresponding to logical operations + XOR +, - XOR - of Table I and 1 XOR 1 of Table II for the central channel. (e) Intensity cross-sections along the coloured dashed lines of images (a)-(d). All images show intensity on the same grayscale.

shift will result in their in-phase interaction with the absorber. The result is an intensity-modulated data stream A XNOR B. Furthermore, the inverse and identity operations can be realized by using the unmodulated carrier as channel B (e.g. corresponding to a fixed + state, see first and third row of Table I) and setting the phase shift between channels A and B to be either $\theta_{ext} = 0$ or π, resulting in conversion of the phase-modulated data stream A into an intensity-modulated data stream NOT A or A, respectively. Logical operations on the central channel do not affect the peripheral channels. Fig. 4 shows — for the same set of 5 A-channels (first column) — how different combinations of B-channels (second column) can

TABLE I. Logical operations between equal intensity phase-modulated data streams A and B ($I_A = I_B = 1$) according to equation (1)

Input states		Output intensities $I_C = I_D$	
		$\theta_{ext} = 0$	$\theta_{ext} = \pi$
A	B	A XOR B	A XNOR B
+	+	0	1
+	-	1	0
-	+	1	0
-	-	0	1

be used to perform logical operations (third and fourth columns) on corresponding combinations of information channels (panels a-c).

Similarly, elementary coherent logical operations can also be realized between coherent intensity-modulated channels[33]. In this case, the phase difference θ between waves interacting on the metasurface is the phase θ_{ext} that is externally imposed between the channels to set the logical operation, $\theta = \theta_{ext}$ (as $\theta_{data} = 0$ in all cases). When the input channel intensities are both zero, the output channel will of course also be zero, while for absorber illumination by a single input channel of intensity 1, the detected intensity will be 0.25 for an ideal planar absorber which will transmit as well as reflect 25% of the incident intensity. However, for simultaneous illumination by both input channels, the detected channel intensity will be strongly phase-dependent, due to perfect absorption for $\theta_{ext} = 0$ (Fig. 3d, e), transparency for $\theta_{ext} = \pi$ (Fig. 3c, e) and partial absorption at intermediate phases. By selecting the correct external phase, we can achieve a range of logical operations. The resulting output channel intensities are listed in Table II and correspond to logical operations A XOR B when θ_{ext} is chosen to be 0 and the threshold is chosen to be a value between 0 and 0.25, A AND B ($\theta_{ext} = \pi$, threshold > 0.25) and A OR B ($\theta_{ext} = \pi/3$, threshold < 0.25), where the suitably chosen threshold intensity separates the logical 1 and 0 states. Real applications may require a further 4× amplification step following the XOR and OR operations to restore the original signal level and to avoid different threshold intensities. An inversion, NOT A, for an intensity-modulated channel A can also be realized for $\theta_{ext} = 0$ by keeping the B-channel switched on. Fig. 4 illustrates coherent logical operations between different combinations of channels, where the third column corresponds to the AND operation, while the fourth column corresponds to the XOR operation. No evidence of crosstalk between neighboring channels has been observed, indicating that our spatial channels are sufficiently well separated to ensure that logical operations between pairs of A- and B-channels are not affected by their neighbours.

In this proof-of-principle demonstration, we select the B-channels with an intensity mask and modulate their phase with the same phase modulator. In applications, it would be desirable to control the phase of each B-
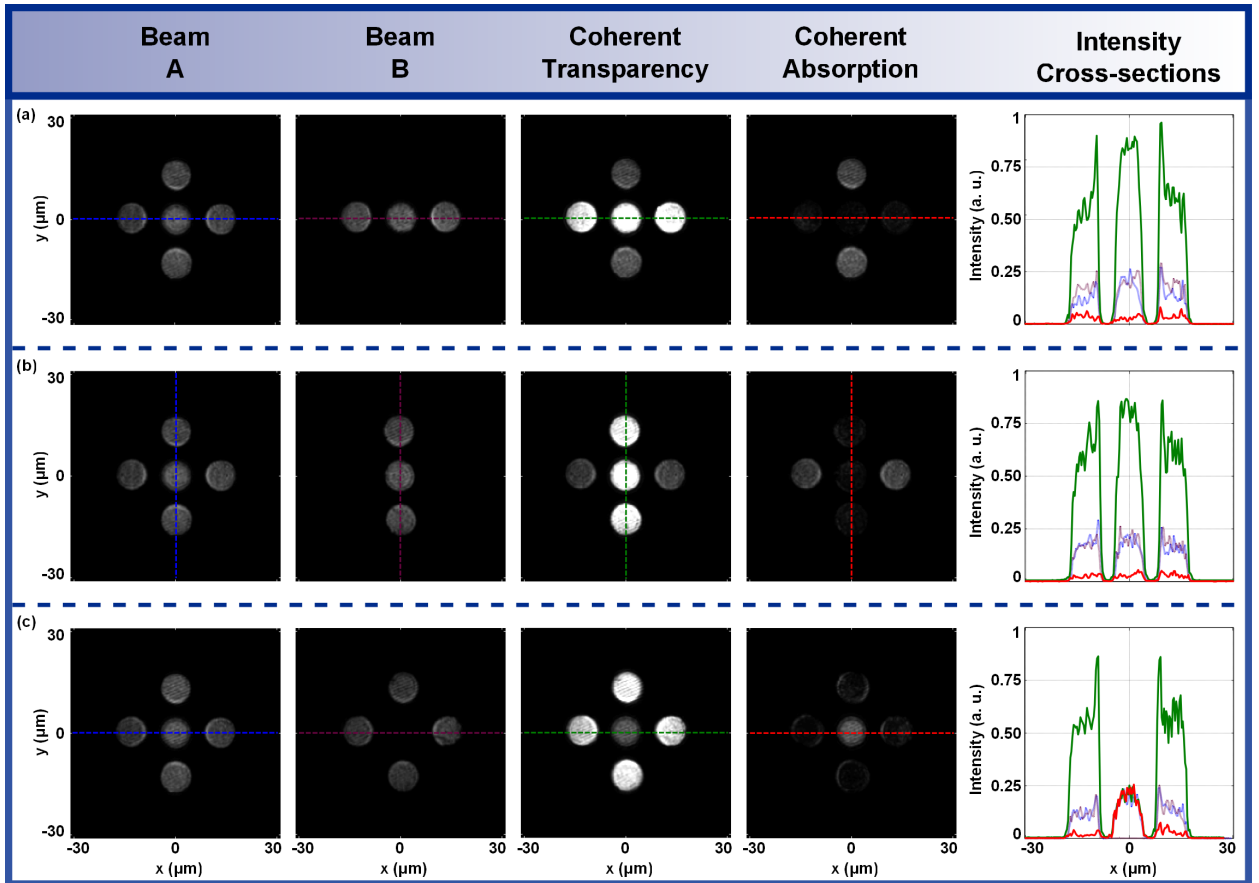
FIG. 4. **All-optical multichannel logic operations.** Images of a metasurface illuminated by a 5-channel signal as beam A (first column) and beams B (second column) corresponding to (a) the horizontal, (b) vertical and (c) peripheral channels. The third and fourth columns correspond to destructive (coherent transparency) and constructive (coherent absorption) interference of beams A and B on the metasurface, respectively. For phase-modulated optical signals (Table I), the third (fourth) column corresponds to the XOR operation between opposite (same) phase states in the selected channels. For intensity-modulated signals (Table II), the third column corresponds to the AND operation, while the fourth column corresponds to the XOR operation. The relative mask alignment is adjusted for each pair of beams A and B. An intensity reduction towards the outer edge of the channel patterns is caused by the Gaussian intensity profile of the beams illuminating the masks. All images show intensity on the same grayscale and the last column shows intensity cross-sections along the dashed lines in images of the same row using corresponding colours.

TABLE II. Logical operations between in-phase ($\theta_{\text{data}} = 0$) intensity-modulated data streams A and B according to equation (1)

Input states		Output intensities $I_C = I_D$		
		$\theta_{\text{ext}} = 0$	$\theta_{\text{ext}} = \pi$	$\theta_{\text{ext}} = \pi/3$
A=I_A	B=I_B	A XOR B	A AND B	A OR B
1	1	0	1	0.25
1	0	0.25	0.25	0.25
0	1	0.25	0.25	0.25
0	0	0	0	0

channel independently. This would allow prescription of different logical operations to each pair of data channels, which could then be switched dynamically. Independent phase control over each B-channel would also enable spatial demultiplexing of arbitrary combinations of information channels. To achieve this, information channels containing the same data stream would be combined on the absorbing thin film, where a constant phase difference $\theta_{\text{ext}} = \pi$ would be applied to wanted information channels to eliminate absorption, while a phase difference of $\theta_{\text{ext}} = 0$ would be set for the unwanted channels, resulting in their complete absorption.

It is important to consider the fundamental energy costs associated with the logical operations and demultiplexing applications discussed above. Spatial demultiplexing and logical operations that convert phase-modulated data into intensity-modulated data — XOR, XNOR, NOT and identity, see Table I – exploit coherent perfect transparency to achieve a logical "1" and coherent perfect absorption to achieve a logical "0", with about 17 dB contrast in our experiments. There are no

unwanted losses in this case. The energy costs associated with logical operations on intensity-modulated data — as shown by Table II – are less favorable. The XOR, OR and NOT operations achieve 11 dB experimental contrast but suffer from 6 dB loss arising from partial absorption of a single input channel. These losses could be reduced to 3 dB by combining the identical output channels C and D and fully compensated by amplification. The AND operation yields a logical "1" (theoretically without any loss) based on coherent perfect transparency, however, imperfect absorption of a single light beam limits the intensity contrast between the "0" and "1" states to 6 dB.

Looking towards implementation of logical operations and demultiplexing in real telecommunications systems, we note that the spectral position of the metamaterial's bands of operation (absorption bands) approximately scales with the size of its unit cell and with the refractive index of the metamaterial's environment. Our metamaterial has absorption bands around 875 nm and 1850 nm wavelength. Thus, a 20% smaller metamaterial structure may be expected to come close to the ideal 50% absorption in the telecommunications band around 1550 nm wavelength, while the existing metamaterial design surrounded by glass (at the interface between two optical fibers) should perform well in the 1310 nm telecommunications band. It is anticipated that any implementations would either involve metamaterial fabrication on optical fiber end faces or encapsulated units with fiber connectors containing lenses that image the fiber output onto a metamaterial. The simulated optical channels investigated here have a diameter of about 9 μm on the metamaterial, which is comparable to typical optical fiber cores. The channel pitch of about 15 μm would need to be increased for typical multi-core fibers that have a core pitch of several 10s of μm. Absence of cross-talk between realistically sized channels with comparatively small spacing indicates that cross-talk between channels will not be an issue for coherent all-optical data processing in multi-core fiber systems. The channels remain well-separated with clearly defined edges, indicating absence of long-range coupling between the split ring apertures of the plasmonic metamaterial. We note that cross-talk between even more closely packed channels or overlapping channels as in spatial mode multiplexing could be explored in future work.

It is important to underline the role of beam splitters in optics and to consider the distinction between lossless and lossy beam splitters in optical networks. Beam splitters are fundamental components of photonic systems, allowing optical information merging in a strictly defined fashion. In quantum optics, beam splitters serve as key components for linear optical quantum computing[34] and combine single photons into exotic N00N states[35]. Recently, exotic properties of lossy beam splitters, such as apparent nonlinear absorption[36], have attracted the attention of the nanophotonics community[29,37]. As illustrated by Fig. 1(a), the interaction of two coherent beams of equal intensity on an "ideal" lossy beam splitter re-

sults in two output beams of equal intensity. In contrast, a lossless beam splitter divides the power unevenly between the output channels. Therefore, the power in a given channel of a coherent optical network can double with every interaction on a lossless beam splitter. Such exponential growth — that can concentrate the power of all input channels in a single output channel and cause equipment overload — is impossible in a coherent network based on the ideal lossy beam splitter, for which the power in any output channel cannot exceed the single channel input power.

We note that the step from single-channel to multichannel logical operations as reported here is non-trivial and technically demanding. Single-channel logical operations can be realized through interaction of two counter-propagating coherent plane waves on a small absorber. In contrast, our implementation of multichannel logical operations engages waves with a continuous spectrum of wave vectors for imaging of multiple channels onto a much larger metasurface area. As coherent absorption is controlled by the phase difference between A and B-channels, phase distortions across all channels must be avoided. This requires flatness within 10s of nm and homogeneity of the plasmonic absorber and of all optical components across the area occupied by all channels, as well as precise alignment.

In summary, we demonstrate how the coherent interaction of light with light on an absorbing beam splitter of substantially subwavelength thickness could be used for dynamic selection and deletion of spatially distinct optical data channels, as well as elementary multichannel all-optical data processing. For example, the XOR operation is a vital component of many all-optical cryptography schemes[38,39]. The speed at which different logical operations can be set and channels selected is in principle set by the response time of commercial phase modulators (10s of GHz). It has been shown by Refs. 19 and 20 for similar arrays of asymmetrically split ring apertures in gold that the speed of the underlying coherent interaction is limited by the plasmon relaxation time to about 10 fs, which is about 3 orders of magnitude faster than telecommunications data rates that are on the order of 10s of Gbit/s per channel. Furthermore, the coherent effect is compatible with arbitrarily low intensities[29]. Therefore, we argue that coherent control of light with light has potential applications in space division multiplexing and elementary all-optical data processing in coherent information networks.

[1] D. J. Richardson, J. M. Fini, and L. E. Nelson, Nature Photon. **7**, 354 (2013).

[2] P. J. Winzer, Nat. Photon. **8**, 345 (2014).

[3] R.-J. Essiambre, R. Ryf, N. K. Fontaine, and S. Randel, IEEE Photon. J. **5**, 0701307 (2013).

[4] T. Mizuno, H. Takara, K. Shibahara, A. Sano, and Y. Miyamoto, J. Lightwave Technol. **34**, 1484 (2016).

[5] T. Hayashi, T. Taru, T. Nagashima, O. Shimakawa, T. Sasaki, and E. Sasaoka, SEI Technical Rev. **77**, 14 (2013).

[6] W. L. Chan, H.-T. Chen, A. J. Taylor, I. Brener, M. J. Cich, and D. M. Mittleman, Appl. Phys. Lett. **94**, 213511 (2009).

[7] C. M. Watts, D.Shrekenhamer, J. Montoya, G. Lipworth, J. Hunt, T. Sleasman, S. Krishna, D. R. Smith, and W. J. Padilla, Nat. Photon. **8**, 605 (2014).

[8] P. Cencillo-Abad, E. Plum, E. T. F. Rogers, and N. I. Zheludev, Opt. Express **24**, 18790 (2016).

[9] Q. Wang, E. T. F. Rogers, B. Gholipour, C.-M. Wang, G. Yuan, J. Teng, and N. I. Zheludev, Nature Photon. **10**, 60 (2016).

[10] M. Papaioannou, E. Plum, J. Valente, E. T. Rogers, and N. I. Zheludev, Light. Sci. Appl. **5**, e16070 (2016).

[11] S. Thongrattanasiri, F. H. L. Koppens, and F. J. García de Abajo, Phys. Rev. Lett. **108**, 047401 (2012).

[12] M. I. Stockman, S. Faleev, and D. J. Bergman, Phys. Rev. Lett. **88**, 67402 (2002).

[13] B. Gjonaj, J. Aulbach, P. Johnson, A. Mosk, L. Kuipers, and A. Lagendijk, Nat Photonics **5**, 360 (2011).

[14] W. J. Wan, Y. D. Chong, L. Ge, H. Noh, A. D. Stone, and H. Cao, Science **331**, 889 (2011).

[15] Z. P. Li, S. Zhang, N. J. Halas, P. Nordlander, and H. Xu, Small **7**, 593 (2011).

[16] J. W. Yoon, G. M. Koh, S. H. Song, and R. Magnusson, Phys. Rev. Lett. **109**, 257402 (2012).

[17] J. Zhang, K. MacDonald, and N. I. Zheludev, Light Sci. Appl. **1**, e18 (2012).

[18] E. Plum, K. Tanaka, W. T. Chen, V. A. Fedotov, D. P. Tsai, and N. I. Zheludev, J. Opt. **13**, 055102 (2011).

[19] X. Fang, M. L. Tseng, J. Y. Ou, K. F. MacDonald, and D. P. Tsai, Appl. Phys. Lett. **104**, 141102 (2014).

[20] V. Nalla, S. Vezzoli, J. Valente, S. Handong, and N. I. Zheludev, CLEO/Europe-EQEC, Munich, Germany (2015).

[21] U. Efron, *CRC Press* (1994).

[22] P. Günter, Phys. Rep. **93**, 199 (1982).

[23] X. Xu, H. Liu, and L. V. Wang, Nat. Photon. **5**, 154 (2011).

[24] M. B. Klein, Opt. Lett. **9**, 350 (1984).

[25] E. Voit, M. Z. Zha, P. Amrhein, and P. Gunter, Appl. Phys. Lett. **51**, 2079 (1987).

[26] J. a. Herlocker, K. B. Ferrio, E. Hendrickx, B. D. Guenther, S. Mery, B. Kippelen, and N. Peyghambarian, Appl Phys Lett **74**, 2253 (1999).

[27] S. A. Mousavi, E. Plum, J. Shi, and N. I. Zheludev, Sci. Rep. **5**, 8977 (2015).

[28] J. Shi, X. Fang, E. T. Rogers, E. Plum, and K. F. MacDonald, Opt. Express **22**, 21051 (2014).

[29] T. Roger, S. Vezzoli, E. Bolduc, J. Valente, J. J. F. Heitz, J. Jeffers, C. Soci, J. Leach, C. Couteau, N. I. Zheludev, and D. Faccio, Nat. Commun. **6**, 7031 (2015).

[30] M. Pu, Q. Feng, M. Wang, C. G. Hu, C. Huang, X. Ma, Z. Zhao, C. Wang, and X. Luo, Opt. Express **20**, 2246 (2012).

[31] S. Li, J. Luo, S. Anwar, S. Li, W. X. Lu, Z. H. Hang, Y. Lai, B. Hou, M. Shen, and C. Wang, Phys. Rev. B **91**, 220301(R) (2015).

[32] E. Plum and N. I. Zheludev, "Structured surfaces as optical metamaterials," (Cambridge University Press, 2011) Chap. 4. Chirality and anisotropy of planar metamaterials, pp. 94–157.

[33] X. Fang, K. F. MacDonald, and N. I. Zheludev, Light. Sci. Appl. **4**, e292 (2015).

[34] E. Knill, R. Laflamme, and G. J. Milburn, Nature **409**, 46 (2001).

[35] J. P. Dowling, Contemp. Phys. **49**, 125 (2008).

[36] S. M. Barnett, J. Jeffers, A. Gatti, and R. Loudon, Phys. Rev. A **57**, 2134 (1998).

[37] T. Roger, S. Restuccia, A. Lyons, D. Giovannini, J. Romero, J. Jeffers, M. Padgett, and D. Faccio, Phys. Rev. Lett. **117**, 023601 (2016).

[38] X. Zhang, W. Li, H. Hu, and N. K. Dutta, J. Opt. Commun. Netw. **7**, 276 (2015).

[39] W. H. Chang, G. C. Yang, C. Y. Chang, and W. C. Kwong, J. Light. Technol. **33**, 1708 (2015).